TISSUE ENGINEERING: Part A
Volume 18, Numbers 1 and 2, 2012

DOI: 10.1089/ten.tea.2011.0301

Original Articles

Initial Binding and Recellularization of Decellularized Mouse Lung Scaffolds with Bone Marrow-Derived Mesenchymal Stromal Cells

Amanda B. Daly, B.S.,[1] John M. Wallis, B.S.,[1] Zachary D. Borg, B.S.,[1] Ryan W. Bonvillain, Ph.D.,[2] Bin Deng, Ph.D.,[3] Bryan A. Ballif, Ph.D.,[3] Diane M. Jaworski, Ph.D.,[4] Gilman B. Allen, M.D.,[1] and Daniel J. Weiss, M.D., Ph.D.[1]

Recellularization of whole decellularized lung scaffolds provides a novel approach for generating functional lung tissue *ex vivo* for subsequent clinical transplantation. To explore the potential utility of stem and progenitor cells in this model, we investigated recellularization of decellularized whole mouse lungs after intratracheal inoculation of bone marrow-derived mesenchymal stromal cells (MSCs). The decellularized lungs maintained structural features of native lungs, including intact vasculature, ability to undergo ventilation, and an extracellular matrix (ECM) scaffold consisting primarily of collagens I and IV, laminin, and fibronectin. However, even in the absence of intact cells or nuclei, a number of cell-associated (non-ECM) proteins were detected using mass spectroscopy, western blots, and immunohistochemistry. MSCs initially homed and engrafted to regions enriched in types I and IV collagen, laminin, and fibronectin, and subsequently proliferated and migrated toward regions enriched in types I and IV collagen and laminin but not provisional matrix (fibronectin). MSCs cultured for up to 1 month in either basal MSC medium or in a small airways growth media (SAGM) localized in both parenchymal and airway regions and demonstrated several different morphologies. However, while MSCs cultured in basal medium increased in number, MSCs cultured in SAGM decreased in number over 1 month. Under both media conditions, the MSCs predominantly expressed genes consistent with mesenchymal and osteoblast phenotype. Despite a transient expression of the lung precursor TTF-1, no other airway or alveolar genes or vascular genes were expressed. These studies highlight the power of whole decellularized lung scaffolds to study functional recellularization with MSCs and other cells.

Introduction

Ex vivo tissue engineering has been successfully utilized for regeneration of tissues, including skin, vasculature, cartilage, bone, and, more recently, heart and liver.[1–3] Given the complex three-dimensional (3D) architecture and structure–function relationships of the lung, this is a potentially difficult daunting task; nonetheless, there has been significant progress in several areas. Synthetic 3D culture systems have recently been used as matrices for *ex vivo* lung parenchymal development and for the study of the effects of growth factors and mechanical forces on lung remodeling.[4–8] Comparable scaffold approaches have been utilized to study creation of pulmonary vascular networks and to investigate effects of vascular endothelial cells on development of airway and alveolar epithelial tissues.[9,10]

Recent work has focused on scaffolds comprised of native trachea, nasal septa, or decellularized whole lungs.[11–19] These are more organotypic scaffolds in which the 3D structure and associated extracellular matrix (ECM) components, including collagens, elastin, and laminin, are left largely intact after removal of cellular material with detergents and other agents. These native scaffolds can then be reseeded with different populations of cells that have recently led to successful clinical use of a bioengineered bronchus.[13] Two recent studies demonstrated that inoculating decellularized whole rat lungs with different mixes of fetal rat lung homogenates, endothelial cells, and A549 carcinoma cells resulted in partial recellularization of the decellularized scaffolds.[18,19] While the resulting cellular architecture did not fully resemble that of native lung, the recellularized lungs were able to be surgically implanted in rats that had previously undergone unilateral pneumonectomy leading to short-term survival of the rats and some restoration of gas exchange and vascular perfusion.[18,19] These are important proof-of-concept studies that are expected to stimulate a number of comparable studies utilizing a variety of decellularized lungs, including human lungs. However, there are few studies as yet evaluating whether embryonic or

[1]Department of Medicine, University of Vermont College of Medicine, Burlington, Vermont.
[2]Center for Stem Cell Research and Regenerative Medicine, Tulane University School of Medicine, New Orleans, Louisiana.
[3]Departments of Anatomy and Neurobiology and [4]Biology, University of Vermont College of Medicine, Burlington, Vermont.

adult stem or progenitor cells can form airway or alveolar-like structures when cultivated in a 3D matrix or whether stem cells cultured as such can be utilized for functional lung regeneration *in vitro* and *in vivo*.

To explore the utility of decellularized whole lung scaffolds as a platform for recellularization with adult stem cells, we first extensively characterized ECM and cell-associated proteins remaining after decellularization of mouse lungs. We subsequently inoculated bone marrow-derived mesenchymal stromal cells (MSCs) into the airways of the decellularized whole mouse lungs, cultured them in either basal MSC media or in small airways growth media (SAGM) over a 1-month period, and investigated their growth and differentiation. To determine potential interactions of the MSCs with ECM proteins remaining in the decellularized lungs, we assessed patterns of initial MSC binding and subsequent growth in spatial relation to collagen types I and IV, fibronectin, laminin, and elastin. Finally, we assessed whether the MSCs themselves might be synthesizing these ECM proteins and potentially contributing to the ECM during recellularization.

Materials and Methods

Mice

Adult male and female C57Bl/6 and BALB/c mice (8–24 weeks, Jackson Laboratories), adult male Sprague-Dawley rats (16 weeks, Jackson Laboratories), and transgenic enhanced green fluorescent protein (eGFP)-expressing mice C57Bl/6-Tg(UBC-GFP)30Scha/J that ubiquitously express enhanced green fluorescent protein (Jackson Laboratories; stock #004353) were maintained at UVM or Tulane University in accordance with institutional and American Association for Accreditation of Laboratory Animal Care standards and review.

Lung decellularization

After euthanasia, heart-lung blocs were removed and the lungs decellularized under sterile conditions over 3 days by sequential instillation and rinsing through both trachea and the right ventricle with distilled water, 0.1% Triton-X100, 2% sodium deoxycholate, 1 M NaCl, and porcine pancreatic DNAse (Sigma) as previously described (see Ref.[16] and Supplementary Methods for detailed protocol; Supplementary Data are available online at www.liebertonline.com/tea). Sham decellularized mouse lungs were prepared using the same protocol with phosphate-buffered saline (PBS)/5× Pen-Strep (Cellgro) substituted for all solutions.

To generate decellularized lung slices, decellularized lungs were filled with agarose, sliced with a sterile razor blade to yield transverse sections of approximately 1 mm in thickness, covered with sterile PBS, and placed at 37°C until agarose melted out of the tissue.

Lung histology and GFP assessment

Lungs were gravity-fixed with 4% paraformaldehyde, embedded in paraffin, and 5-μm sections mounted on glass slides. After deparaffinization, sections stained with hematoxylin and eosin (H&E), Verhoeff's Van Gieson, Masson's Trichrome, Alcian blue, or Alizarin Red S stains were assessed by standard light microscope.[16,20] For assessment of GFP fluorescence the PBS-perfused heart-lung block was removed from GFP-expressing and control C57Bl/6 mice, decellularized as described above, embedded in 100% optimal cutting temperature, and frozen in liquid nitrogen vapor. Mounted (Vectashield mounting medium) 20 μm cryosections were stained with 4′,6′-diamidino-2-phenylindane (DAPI) (Vector Labs) and images captured by fluorescence microscopy with GFP- and DAPI-specific fluorescences observed at exposure times of 1/8 and 1/3 s, respectively.

To assess the percent parenchyma versus airspace in the native versus decellularized lungs, images were taken of 6 random nonoverlapping parenchymal areas of H&E-stained sections from three naive and three decellularized lungs (400× agnification using Olympus BX50 Light Microscope with QImaging Retiga 2000R digital camera) providing 18 images of the naive and decellularized groups, respectively. Percent parenchyma per image was calculated using ImageJ (version 1.43u).

Electron microscopy

Approximately 1 mm^3 pieces of proximal lung, distal lung, and distal trachea were cut from decellularized mouse lungs and were processed according to standard protocol (see Supplementary Methods for details) and examined with a JEOL 1400 TEM (JEOL USA, Inc.) operating at 60 kV.

Immunofluorescence staining

After deparaffinization, immunofluorescent staining was performed according to standard protocols with primary antibodies against Fibronectin, Laminin, Smooth muscle myosin heavy chain 2, Elastin, Collagen I, Collagen IV, Ki67, Cleaved Caspase-3, and Actin (see Supplementary Methods for full protocol and reagent details).

Mass spectrometry

Six samples (three pieces each from two separate decellularized lungs, approximately 25 μg for each sample) were processed according to standard protocol (see Supplementary Methods for details) and loaded onto a fused silica microcapillary LC column packed with C18 reversed-phase resin. Peptides were separated at a flow rate of 250 nL/min for 45 min. Nanospray ESI was used to introduce peptides into a linear ion trap quadrupole mass spectrometer (Thermo Electron). Mass spectrometry (MS) data were acquired in a data-dependent acquisition mode, in which a full MS scan was followed by 10 MS/MS scans of the most abundant ions.

After an LC-MS run was completed and spectra obtained, the spectra were searched against the IPI Mouse protein sequence databases (V 3.75) using SEQUEST (Bioworks software, version 3.3.1; Thermo Electron), with search parameters detailed in Supplementary Methods. Proteins that were identified by two or more peptides in each of the six samples were compiled and are presented in Table 1. Proteins presented in Table 1 are broadly categorized and ranked by the average number of peptides identified from the six samples.

Western analyses

Western blot analysis was performed as previously described (see Ref.[21] and also Supplementary Methods) with antibodies against actin, collagen type I, collagen type IV, elastin, fibronectin, glyceraldehyde 3-phosphate dehydrogenase, histone H1, laminin, and smooth muscle myosin. After washing, blots

Table 1. Mass Spectrometric Analysis of Residual Proteins in De-Cellularized Mouse Lungs

Protein ID	*Protein description*	*Peptides identified*
Extracellular matrix proteins		
COL6A3	Collagen type VI alpha 3	26
HSPG2	Heparan sulfate Proteoglycan 2 (perlecan)	21
LAMA	Laminin alpha	13
LAMB2	Laminin beta 2 (laminin S)	12
LAMC1	Laminin gamma 1	12
COL4A2	Collagen (IV) chain	10
Cytoskeletal proteins		
ACTB	Actin, beta, cytoplasmic	37
ACTG2	Actin, gamma 2	36
ACTA2	Actin, alpha 2	36
ACTC	Actin, alpha	36
ACTA1	Actin, alpha	35
ACTG1	Actin, gamma	34
TUBB2C	Tubulin beta 2C	28
ACTBL2	Beta-actin	24
TUBB4	Tubulin beta 4	23
TUBB2A	Tubulin beta 2A	22
TUBB2B	Tubulin beta 2B	22
TUBA6	Tubulin alpha 6	20
TUBB5	Tubulin beta 5	20
TUBA8	Tubulin alpha 8	16
TUBB3	Tubulin beta 3	16
TUBB6	Tubulin beta 6	9
TUBB1	Tubulin beta 1	5
Cytoskeletal-associated proteins		
MYH9	Myosin heavy polypeptide 9	43
MYH14	Myosin heavy polypeptide 14	33
TLN1	talin 1	31
MYH10	Myosin heavy polypeptide 10	26
MYH11	Myosin heavy polypeptide 11	18
SPTBN1	Spectrin beta	14
VIM	Vimentin	14
FLNA	Filamin-A	13
SPNA	Spectrin alpha	12
MYH6	Myosin heavy polypeptide 6	9
MYH1	Myosin IC	8
VCL	Vinculin	7
ACTN1	Actinin alpha 1	7
ACTN4	Actinin alpha 4	5
CRMP2	Collapsin response mediator protein 2	5
PLEKHC1	Pleckstrin homology domain containing family C member 1	4
Other proteins		
HIST2H4	Histone H4	27
CLTC	Clathrin, heavy polypeptide (Hc)	15
HIST1H2B	Histone H2b	15
HISTH3	Histone H3	13
EHD2	EH-domain containing 2	11
EEF1A1	Eukaryotic translation elongation factor 1	10
ANXA2	annexin A2	8
IQGAP1	IQ motif containing GTPase activating protein 1	7
TGM2	Transglutaminase 2 C polypeptide	6
EEF2	Eukaryotic translation elongation factor 2	6
ALDH2	Aldehyde dehydrogenase 2	5
EHD4	EH-domain containing 4	4

were incubated with species-specific horseradish peroxidase-conjugated secondary antibodies and immunoreactive species identified using enhanced chemiluminescence (PerkinElmer Life Sciences). Densitometry was performed using Quantity One software (Bio-Rad).

Perfusion studies

Mouse and rat lungs were decellularized as described above. In mice, the right ventricle was cannulated; in rats the pulmonary artery and left atrium were cannulated. About 1.5% Evans Blue dye was injected through the right ventricle or pulmonary artery with continuous video recording obtained using a Sony Cybershot W330 digital camera and sequential still images captured from the video.

Lung mechanics

Extracted lungs were intubated with an 18 gauge metal cannula, connected to a flexiVent mechanical ventilator (SCIREQ), and ventilated according to a standard protocol elaborated in the Supplementary Methods.[22] Respiratory impedance (Zrs) was determined and interpreted by being fit to the constant phase model of the viscoelastic lung, from which were derived values for tissue elastance (*H*), a parameter reflecting the combined effects of tissue stiffness and surface tension at the air-liquid interface of the lung.[23,24]

Cells and cell inoculation

MSCs derived from bone marrow of adult male C57Bl/6 mice were obtained from the National Center for Research Resources/National Institute of Health Center for Preparation and Distribution of Adult Stem Cells at Tulane University.[20] C10 mouse lung epithelial cells were obtained courtesy of Matthew Poynter (University of Vermont).[25] MSCs were cultured following standard protocol (see Supplementary Methods). Purity was determined by expression of Sca-1, CD106, CD29, absence of CD11b, CD11c, CD34, and CD45 expression, and the ability to differentiate into osteoblasts, chondrocytes, and adipocytes *in vitro*.[20] C10 cells were cultured under standard conditions.[25]

To seed each decellularized lung, 2×10^6 MSCs suspended in 3 mL MSC basal medium were administered by intratracheal inoculation and the lungs were submerged overnight in basal MSC media at 37°C and 5% CO_2. The next day, the medium was changed to either fresh basal medium or to SAGM[25] (see Supplementary Methods for detailed media formula). The inoculated lungs were then cultured for 1, 3, 7, 14, or 28 days with lungs immersed in fresh medium every 2 to 3 days. At each time point, three seeded lungs were harvested for histological analysis and 3 seeded lungs were harvested for RNA extraction. Lungs were similarly seeded with C10 cells in C10 basal media.[25]

For integrin blocking studies, cells cultured following standard protocol were lifted from tissue culture plastic using 1× Versene (Gibco) to keep extracellular proteins intact. The cells were counted and resuspended to a concentration of 1×10^6 cells/mL in PBS–2% fetal bovine serum (FBS). α5 Integrin on MSCs was blocked by adding purified rat anti-mouse CD49e (5H10-27; BD Pharmingen) to cell suspension at a concentration of 10 μg/mL for 30 min at room temperature. The decellularized lung tissue was blocked by instilling basal medium (10% FBS) into lung and incubating for

20 min at room temperature under sterile conditions. Cell suspension was washed twice with 2 mL of PBS–2% FBS.

Blocked MSCs were seeded into a single lobe of the decellularized lung in 3 mL MSC basal medium via intratracheal inoculation and the lung lobe was submerged overnight in basal MSC media at 37°C and 5% CO_2. The next day lungs were harvested for histological and immunofluorescent analyses as described.

Genomic DNA isolation

Naive and decellularized lungs were digested and DNA was precipitated and pelleted using a protocol detailed in the Supplementary Methods. The dry DNA pellet was resuspended in 100 μL of nuclease-free water. DNA was quantified on a Nanodrop spectrophotometer, and equal amounts were loaded into a 1.5% Agarose (Invitrogen) gel. DNA bands were observed with ethidium bromide under UV conditions.

RNA extraction

Heart and tracheal tissue was removed from seeded lungs by dissection. Isolated lung tissue was then submerged in 1 mL TRIREAGENT reagent (Molecular Research Center Inc.) and, after homogenization, RNA was extracted following the manufacturer's instructions, then cleaned using PrepEase columns (USB), and eluted in 60 μL nuclease-free water (see Supplementary Methods for greater detail). Total RNA purity and concentration were assessed by spectrophotometery via Nanodrop.

Quantitative polymerase chain reaction

Equal amounts of total RNA from each sample were used as template for cDNA synthesis and amplification performed with an iScript cDNA Synthesis Kit (Bio-Rad) according to manufacturer's instructions. All reverse transcriptase (RT)-quantitative polymerase chain reaction (qPCR) was performed using IQ-SYBR Green Supermix (Bio-Rad) according to manufacturer's instructions. Lung-specific primer sets used were AQP5, CFTR, SPC, TTF1, aENaC, CK18, and ZO1. Fibroblast-specific primer sets used were aSMA, Col1a1, and FN1. Endothelial-specific primer sets used were PECAM, TIE1, and TIE2. Cartilage, bone, and adipose tissue-specific primer sets, respectively, were Col2a1, Osteop, and Adipoq. Primer set sequences are found in the Supplementary Methods. Baseline mouse (m)MSC control was obtained

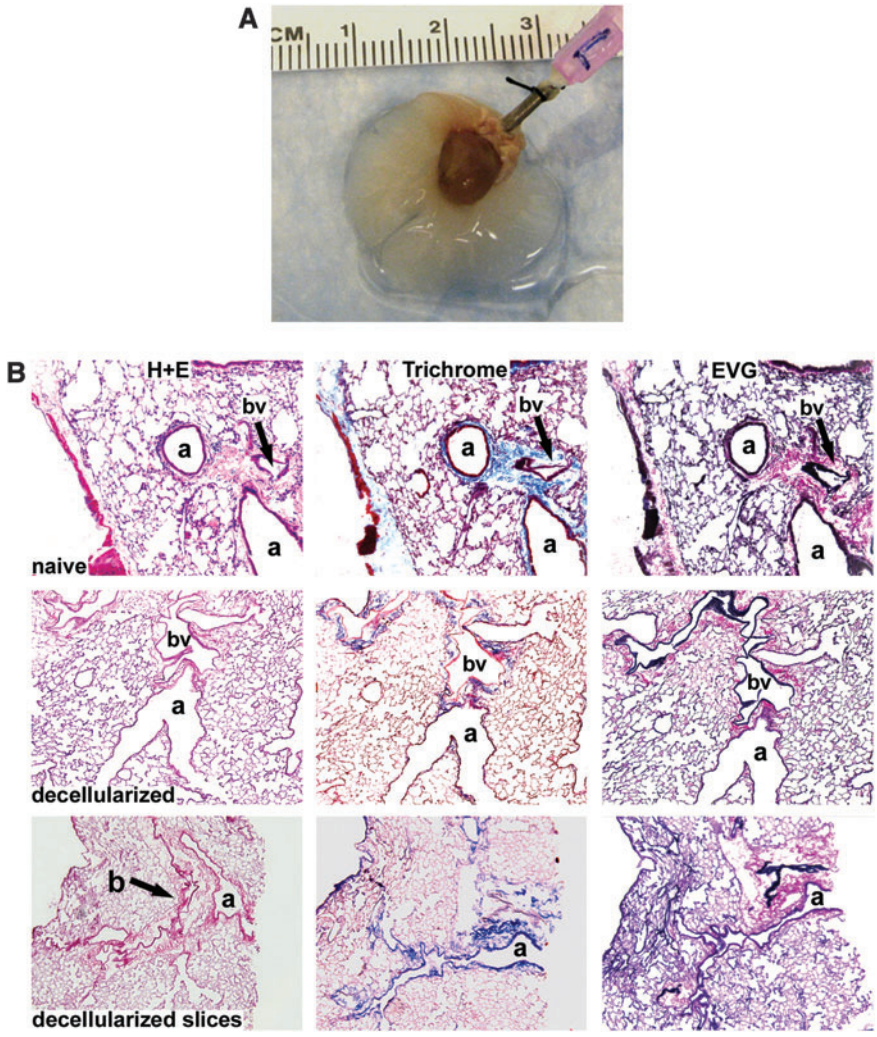

FIG. 1. Histologic assessment of decellularized whole mouse lungs and lung slices demonstrates preservation of normal architecture. **(A)** Whole decellularized heart-lung bloc. The trachea is cannulated with a 18 gauge blunted needle. **(B)** H&E, Masson's Trichrome collagen, and Verhoeff's Van Gieson staining of native lungs, decellularized whole lungs, and approximately 1-mm-thick slices of decellularized lungs. Original magnifications: 100×. a, airway; bv, blood vessel. **(C)** Percent parenchyma in native versus decellularized lungs. Means ± standard error of three lungs assessed for each experimental condition are shown. **(D)** Transmission electron micrograph images of different regions of a representative decellularized whole mouse lung are shown. Original magnifications **(A)** 600×, **(B)** 1000×, **(C)** 1000×, **(D)** 3000×. **(E)** Total DNA content of a native C57Bl/6 mouse lung versus two representative decellularized whole lungs. **(F)** Demonstration of residual RNase but not DNAse activities in decellularized whole lungs. DNA and RNA ladders are shown in the first column (−). Ladders with addition of either DNAse or RNAse are shown in the second column as positive controls. Two different representative native lungs and decellularized lungs are shown for comparison. H&E, hematoxylin and eosin. Color images available online at www.liebertonline.com/tea

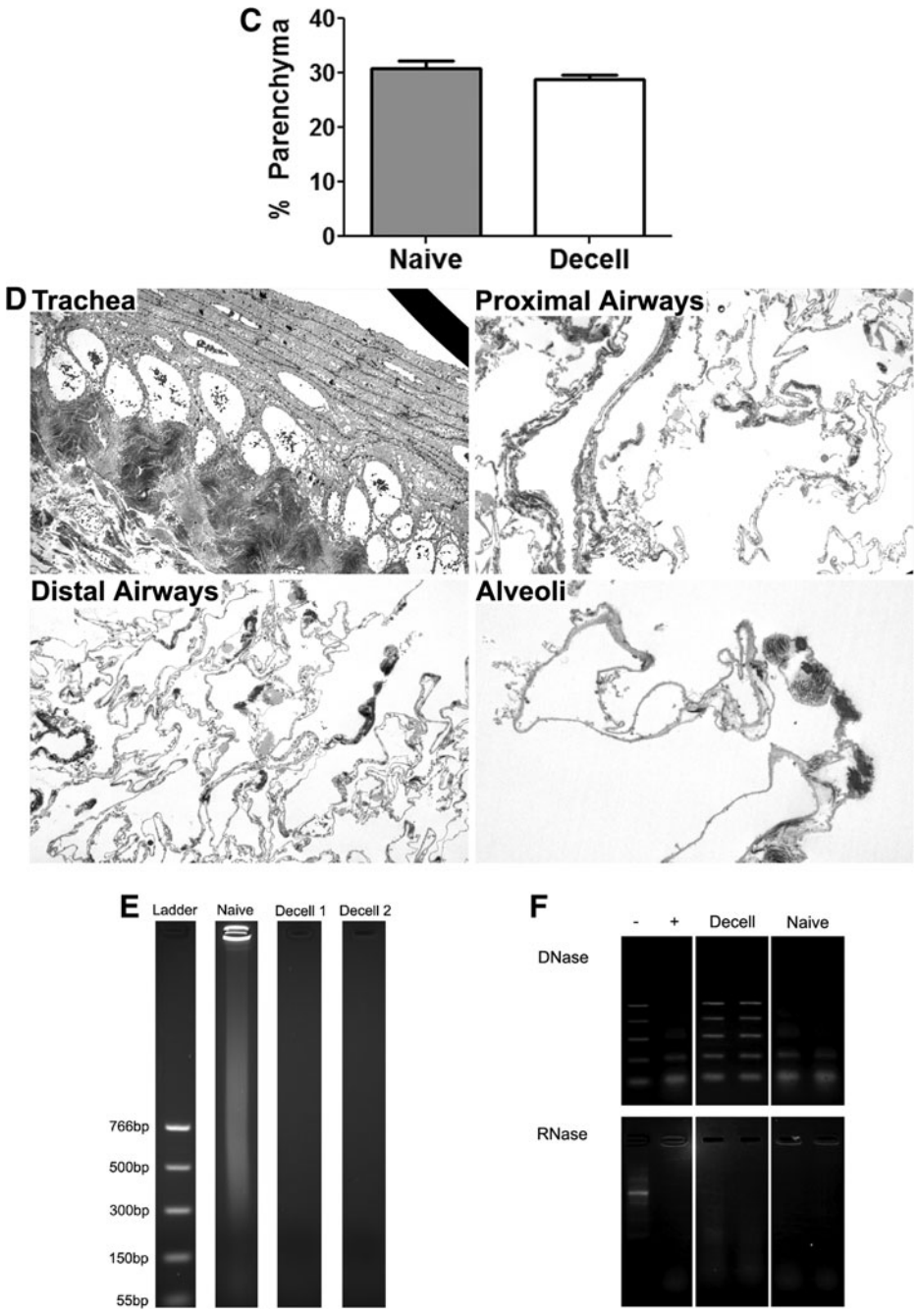

FIG. 1. (Continued).

from mMSCs grown in standard tissue culture conditions. Baseline lung control was obtained a whole lung homogenate from an adult (12 week) female C57Bl/6 mouse.

DNAse and RNAse assessment

Decellularized lungs were homogenized and the resulting supernatant was mixed with PCR buffer (1×), $MgCl_2$ (1 mM), DNA or RNA ladder, and nuclease-free water. Positive control tubes contained PCR buffer (1×), $MgCl_2$ (1 mM), DNA or RNA ladder, and DNase I or RNase H. Negative control tubes contained nuclease-free water, PCR buffer (1×), $MgCl_2$ (1 mM), and DNA or RNA ladder. All tubes were incubated in C1000 thermocycler (Bio-Rad) at 37°C for 2 h. Tube contents were run on 2% agarose (Invitrogen) gel containing ethidium bromide and observed under UV conditions. Test was considered valid if positive control tubes showed ladder degradation and negative control tubes showed intact ladder.

Statistical analyses

Differences between percent parenchyma, total RNA, and qPCR results were assessed by unpaired *t*-test.[27] Western blot and measurements of lung elastance were analyzed by one-way analysis of variance (ANOVA) with Bonferroni *post*

hoc analysis and post-test Dunnett or Newman-Keuls multiple comparison analyses performed with Prism software.[21,22] Detailed statistical methods are presented in the Supplementary Methods.

Results

Detailed characterization of decellularized mouse lungs

Several different approaches have recently been utilized to decellularize whole rodent lungs.[15–19] We utilized that of Lwebuga-Mukasa *et al.*[15] as modified by Price *et al.*[16] Similar to their findings, the gross structure of the lungs remained intact after completion of the protocol (Fig. 1A). Histologic evaluation with H&E, Verhoeff's Van Gieson, and Masson's trichrome stains demonstrated absence of intact cells and nuclei throughout the tissue, as well as maintenance of normal airway, vascular, and alveolar architecture (Fig. 1B). Native architecture was also maintained in decellularized lung scaffolds that had been sliced into sections of approximately 1 mm thickness (Fig. 1B). Morphometric assessment of H&E-stained sections of native lungs and decellularized lung scaffolds inflated to equal pressures demonstrated comparable percent parenchyma (Fig. 1C). In some decellularized lungs, some nuclei were observed in the subepithelial regions of the cartilaginous trachea (chondrocytes, data not shown), suggesting that these cells are not always fully exposed to the decellularization reagents. Transmission electron microscopy of the decellularized lungs confirmed preservation of normal architecture (Fig. 1D). No residual DNA was found in the decellularized lung scaffolds (Fig. 1E). Although DNAse was used in the decellularization protocol, no DNAse activity was noted in the decellularized lung scaffolds; however, residual RNAse activity was present (Fig. 1F).

Evaluation of the ECM protein composition by alcian blue staining and by immunofluorescence demonstrated preservation of key ECM proteins, including collagen I, collagen IV, laminin, and fibronectin, but substantial loss of glycosaminoglycan (GAG; Alcian blue staining) and elastin content after decellularization (Fig. 2). Quantitative assessment by western blot of native and decellularized lung homogenates demonstrated absence of the intracellular enzyme glyceraldehyde 3-phosphate dehydrogenase and minimal residual amounts of histone 1, whereas the ECM proteins collagen I, collagen IV, laminin, and fibronectin were enriched as a proportion of the total protein in the decellularized lung scaffolds (Fig. 3A). Sham decellularization, in which PBS was used in place of each reagent, demonstrated no significant change in the relative abundance of collagen I, collagen IV, or laminin, and a decrease in the relative abundance of fibronectin. Relative abundance of elastin was decreased by both full and sham decellularization procedures, suggesting that this ECM protein is particularly labile (Fig. 3A).

To further assess the effects of the decellularization treatment, mass spectrometric analyses were performed on decellularized lungs (Table 1). ECM proteins detected included collagens, fibronectin, and laminin but did not include elastin, commensurate with the immunohistochemistry. Additionally, a number of intracellular proteins were also detected, including myosin and several isoforms of actin and tubulin. However, quantitative assessment by western blot

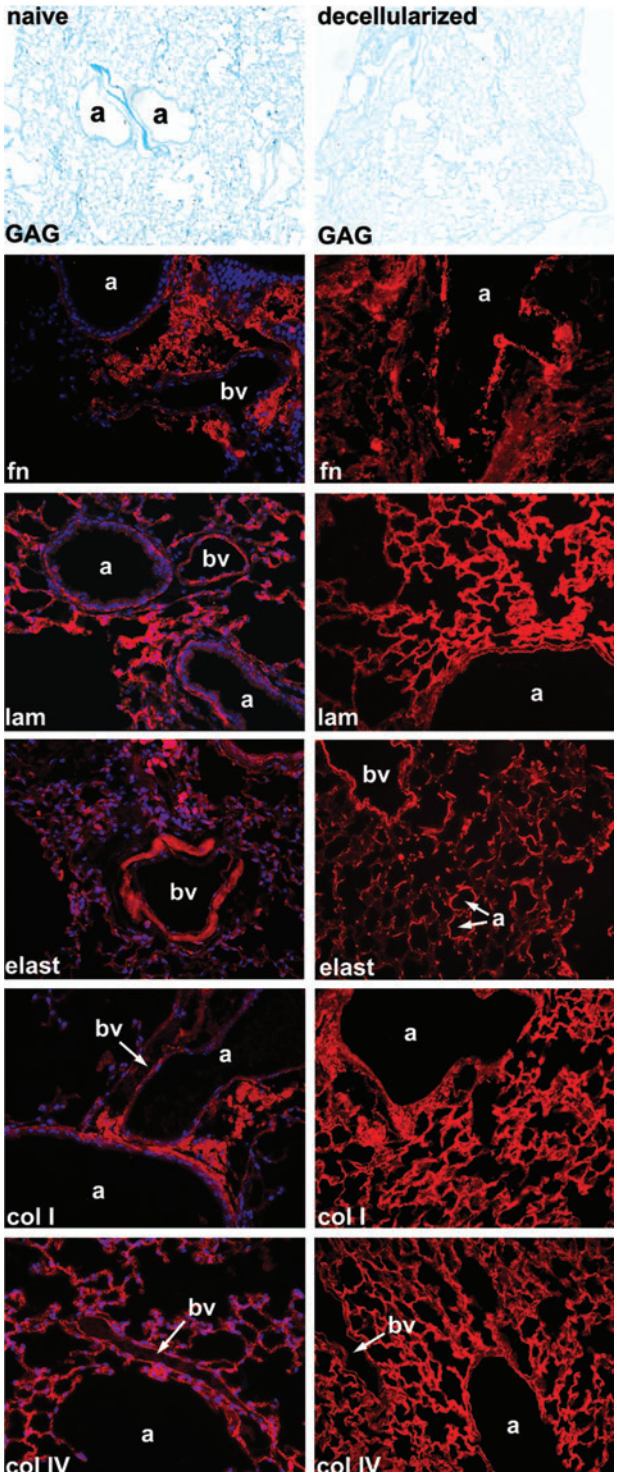

FIG. 2. Immunofluorescent and histologic staining demonstrates retained ECM proteins in whole decellularized lungs. For each set of IF images, the specific ECM protein is shown in red with a DAPI nuclear costain. Glycosaminoglycan content is stained blue with Alcian blue stain. Fn, fibronectin; lam, laminin; elast, elastin; coll, type I collagen; colIV, type IV collagen; a, airway; bv, blood vessel. Representative photomicrographs from a decellularized C57Bl/6 mouse lung are shown. Original magnification 400× for IF photomicrographs and 100× for Alcian blue photomicrographs. ECM, extracellular matrix; IF, immunofluorescent; DAPI, 4′,6′-diamidino-2-phenylindane. Color images available online at www.liebertonline.com/tea

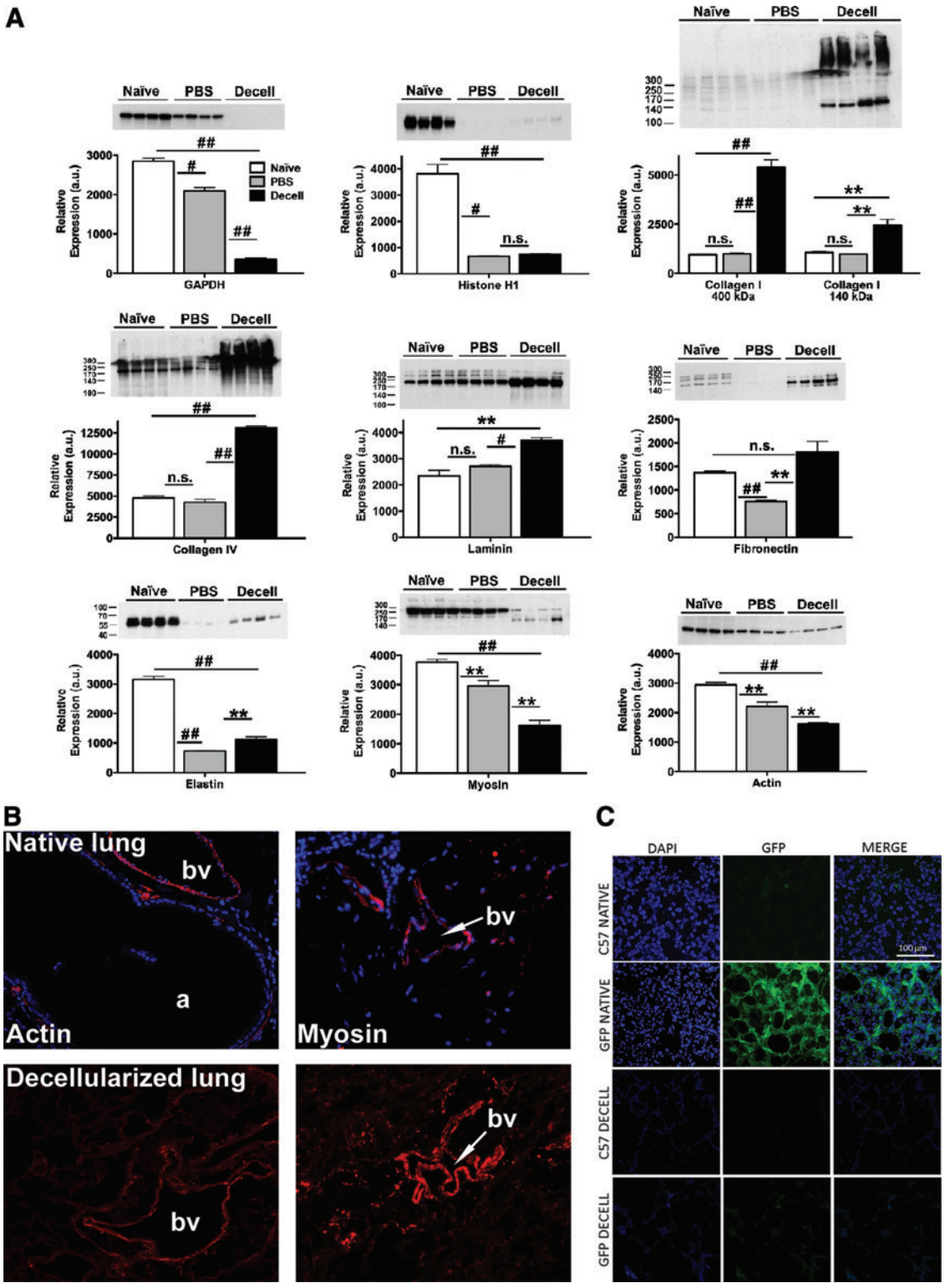

FIG. 3. Intracellular proteins can be detected in decellularized lung homogenates. **(A)** Four representative blots are shown, respectively, for native lungs, lungs sham decellularized with PBS only, and for lungs undergoing full decellularization. Quantitative data are presented as mean ± SEM. Significant interactions were identified by one-way analysis of variance with Bonferroni *post hoc* analysis using Prism software. $^{*}p \le 0.05$, $^{\#}p \le 0.001$, $^{\#\#}p \le 0.0001$, $^{**}p \le 0.01$, n.s., non-significant. **(B)** Representative immunofluorescent staining for smooth muscle actin and smooth muscle myosin heavy chain. Original magnifications = 200×. **(C)** Direct GFP fluorescence in native and decellularized C57Bl/6 and eGFP-expressing mouse lungs. Original magnifications 200×. PBS, phosphate-buffered saline; SEM, standard error of the mean; eGFP, enhanced green fluorescent protein. Color images available online at www.liebertonline.com/tea

demonstrated significant decreases in relative abundance of actin and myosin in decellularized lungs compared with native lungs (Fig. 3A). Immunofluorescent assessment of the decellularized lungs showed residual actin and myosin around some medium- or large-sized blood vessels and some larger airways; this was comparable to the distribution observed in native lung (Fig. 3B). Decellularization of lungs obtained from a constitutive cytosolic eGFP-expressing transgenic mouse demonstrated no retention of GFP fluorescence after decellularization (Fig. 3C).

Perfusion and lung mechanics in decellularized whole mouse lungs

To characterize vascular continuity in the decellularized lungs, 1.5% Evan's blue dye was instilled into the right ventricle (in mouse lungs) or the pulmonary artery (in rat lungs). Rapid diffusion through the vascular tree was observed in both mouse and rat lungs (Fig. 4A) and rapid egress of dye from the left atrium was observed in rat lungs (Fig. 4A, Supplementary Video S1). Measurement of lung mechanics using the forced oscillation technique[22–24] demonstrated a significant increase in lung stiffness, that is, elastance (H) after decellularization (Fig. 4B). Because loss of elastin with decellularization would be expected to reduce lung elastance, we speculated that the observed increase in elastance was due to an overriding net increase in surface tension due to the loss of surfactant during the decellularization process. We subsequently found that instillation of surfactant into the decellularized lung partly restored overall lung compliance (i.e., reduced elastance; Fig. 4B). *Post hoc* means comparisons demonstrated significant differences in mean baseline (post-deep inflation [DI]) lung elastance values between all the groups (ANOVA, $p < 0.05$) except when comparing lavaged lungs to decellularized lungs with surfactant. The total increase in elastance over each 8 min measurement period (ΔH) was significantly greater in the lavaged lung compared with the intact and decellularized lung (ANOVA, $p < 0.05$).

Growth and differentiation of MSCs in decellularized whole lungs

To assess the ability of mouse bone marrow-derived MSCs to adhere to and subsequently proliferate and differentiate in the decellularized lungs, MSCs were inoculated by intratracheal injection (2×10^6 cells/lung) and cultured for up to 1 month in either basal MSC media or in SAGM. The inoculated MSCs appeared to thrive, predominantly in parenchymal regions (Fig. 5A) but also in smaller numbers along both large and small airways after culture in either basal media or in SAGM (Fig. 5B). Several different morphologies were observed in cells growing in parenchymal regions, including both rounded and flattened elongated cells (Fig. 5A). There was no obvious difference in morphologies in parenchymal cells cultured in basal media or SAGM. Cells growing along airways remained flattened and squamous in appearance and no cells of pseudostratified polarized ciliated or nonciliated epithelial appearance were observed. While the number of cells on histologic sections were not quantified due to the stochastic nature of the inoculation process, the total number of cells appeared to increase over 1 month in basal MSC medium; these cells showed continued proliferation as assessed by Ki67 staining (Fig. 5C) and increasing amounts of total RNA over time (Fig. 5D). In contrast, the numbers of cells cultured in SAGM

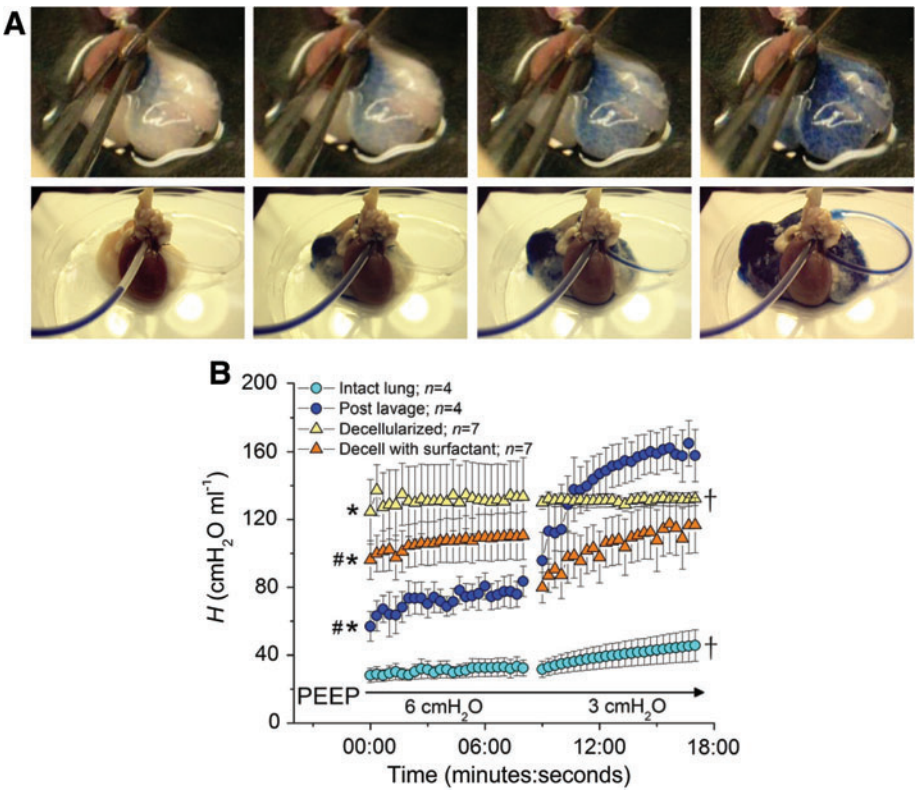

FIG. 4. Vascular perfusion is preserved and lung elastance increased in whole decellularized mouse lungs. **(A)** Sequential images of dye perfusion in mouse (top panel) and rat (bottom panel) lungs. **(B)** Mean values for lung elastance (±SEM) measured at PEEP of 6 and 3 cm H_2O, plotted against time, in intact native lungs, then after saline lavage, and then after decellularization and intratracheal instillation of surfactant (into decellularized lungs). * indicates that baseline mean lung elastance is significantly greater than that of the intact lung ($p \leq 0.05$), # indicates that baseline mean lung elastance is significant less than that of the decellularized lung ($p \leq 0.05$), † indicates that ΔH is significantly less than that of the lavaged lung ($p \leq 0.05$). PEEP, positive end-expiratory pressure. Color images available online at www.liebertonline.com/tea

appeared to decline over the 1 month period after inoculation, with decreasing amounts of whole lung total RNA (Fig. 5D) in spite of continued proliferation as assessed by Ki67 staining (Fig. 5C). No significant early apoptosis, as assessed by caspase-3 staining, was observed in cells cultured in either basal media or in SAGM at any time point (data not shown).

To assess potential differentiation of the MSCs cultured either in basal media or in SAGM, inoculated lungs were assessed by RT-qPCR for mRNA expression of lung epithelial (CCSP, CFTR, pro-SPC, AQP5, αENaC, and CK18), tight junction (ZO-1), endothelial (CD31, Tie1, and Tie2), and fibroblast/myofibroblast (type 1 collagen, αSMA, and fibronectin) genes. Expression of genes characteristic of MSCs differentiating along standard osteoblast, adipocyte, or chondrocyte lineages (osteopontin, adiponectin, and Col2a1) was also evaluated (Fig. 5E). Expression of mRNA for type 1 collagen, α-SMA, and fibronectin was present under most conditions although at levels lower than that of control cultured plastic adherent MSCs. Fibronectin and type 1 collagen mRNA expression increased with longer culture in the decellularized lungs, particularly in basal MSC media. Osteopontin mRNA expression was greater than that of control MSCs and increased over time, particularly in basal media. Alizarin Red staining demonstrated that some of the MSCs cultured for 28 days in either basal MSC medium or in SAGM did have osteoblast phenotype (Fig. 5F). No other mesenchymal or endothelial gene expression was detected. TTF-1 mRNA expression transiently increased at 7 and 14 days of incubation, particularly with culture in SAGM, but decreased at 1 month of incubation. However, no gene expression for epithelial proteins found in native airways or alveoli was detected under any condition, with the exception of ZO-1 mRNA expression, which was detected after 28 days of culture in both basal medium and SAGM. No TTF-1 or ZO-1 mRNA expression was found in control cultured plastic adherent MSCs.

Initial binding and subsequent ECM interactions of MSCs inoculated into decellularized whole lungs

To characterize the initial localization of MSCs in relation to specific ECM proteins and to determine whether the MSCs themselves secrete ECM proteins, decellularized lungs were assessed at 1 and 28 days after inoculation and culture in basal MSC medium (Fig. 6). One day after inoculation, cells were predominantly found in clumps; after 28 days in culture, the cells were spread diffusely through the parenchyma and airways (Fig. 6A). At 1 day in culture, the cells were associated with regions relatively enriched in collagen I, collagen IV, fibronectin, and laminin (Fig. 6B). At 28 days, the MSCs retained their association with regions enriched in collagen 1, collagen IV, and laminin, but fewer MSCs were localized in regions enriched in fibronectin. While little elastin was present in the decellularized lungs, MSCs did not appear to localize in regions in which elastin remained at either 1 or 28 days (Fig. 6B). At both 1 day and 28 days after inoculation, the majority of MSCs themselves were strongly positive by immunofluorescent staining for collagen I, fibronectin, and laminin. Some of the MSCs also stained positively for collagen IV but no cells stained positively for elastin (Fig. 6B).

Intratracheal administration of C10 mouse lung epithelial cells, which express different cell surface integrins than do MSCs and notably do not constitutively express the major fibronectin-binding integrin, $\alpha5\beta1$,[25] results in a different initial distribution pattern (Fig. 6C). Further, incubation of mMSCs prior to intratracheal inoculation with a neutralizing anti-α5 integrin antibody, which blocks binding to fibronectin, inhibits initial mMSC localization to fibronectin-rich areas (Fig. 6C). Use of this antibody also appears to inhibit fibronectin production by the inoculated MSCs (Fig. 6C).

Discussion

In the United States alone, approximately 1000–1500 lung transplants per year are performed, but a significant shortage of suitable donor lungs and the drawbacks of lung transplantation, including lifelong immunosuppression and an approximate 50% 5-year mortality, demonstrates a critical need for new approaches.[28] Unlike cadaveric organs such as kidneys, which have been successfully utilized for many years, transplantation of cadaveric lungs has not been feasible. *Ex vivo* cellularization of 3D scaffolds to produce functional lung tissue has been proposed as an alternative and investigations of synthetic 3D scaffolding as a matrix for such efforts has shown promise.[4–10] For example, culture of fetal rat or mouse lung suspensions grew alveolar-like structures when cultured in a 3D GAG scaffold or synthetic polymer scaffolds.[4,7] Fetal rat lung cells cultured in a biosynthetic gelatin matrix and subsequently injected into normal rat lungs induced formation of branching, sacculated epithelial structures reminiscent of lung parenchymal architecture.[8] Comparable scaffold approaches have been utilized to study creation of pulmonary vascular networks and to investigate effects of vascular endothelial cells on development of airway and alveolar epithelial tissues.[9,10] Recent studies have also demonstrated that matrix protein composition, 3D scaffolds, and mechanical forces can influence differentiation of embryonic stem cells (ESCs) to lung epithelium.[17,29–32] As such, use of different artificial 3D scaffolds is a powerful technique for generating functional lung tissue *ex vivo*.

However, establishment of functional vascular and airway connections remains challenging with artificial scaffolds as they do not fully replicate the complex structure or matrix composition of the lung. In contrast, decellularization of whole cadaveric lungs results in an intact scaffold that largely maintains native airway, alveolar, and vascular architecture, and ECM protein composition.[15–19] Presumably, the decellularization process removes cellular antigens responsible for immune rejection although this has not yet been rigorously tested. These scaffolds can be recellularized with either differentiated adult cells, ESCs, or with adult stem cells, including induced pluripotent stem cells derived from individual patients, and subsequently utilized for autologous transplantation. Further, the decellularized scaffolds can be implanted and functionally connected with both vascular and airway systems.

In the current study, we report decellularization of whole mouse lungs that yields intact 3D scaffolds maintaining many structural features of native lung. We further describe an approach for generating thin slices of decellularized whole lungs that also maintain appropriate structural features. These slices can be utilized for high-throughput evaluations of the effects of various environmental

conditions on growth and differentiation of cells inoculated into the decellularized lungs. Further, vascular continuity is intact in the decellularized whole lung preparations as demonstrated by dye perfusion. This indicates that the lung capillary network remains intact after decellularization, a feature that is difficult to demonstrate with either light or electron microscopy.

As in recent studies of whole lung decellularization that reported model-fitting pressure-volume curves and other measures upon assessment of lung function,[16,18,19] the decellularized lungs in this study were sufficiently leak resistant for analysis of mechanical function using a forced oscillation technique. Notably, we found that the lungs became significantly more stiff once they were decellularized. Although the changes in elastance when going from positive end-expiratory pressure (PEEP) 6 to 3 did not reach statistical significance in any of the groups when analyzed separately, the complete absence of any effect of PEEP on H or ΔH in the decellularized lung was rather unexpected. This unique loss of PEEP dependence in the decellularized lung could simply represent an inability of added PEEP to recruit the lung to any degree whatsoever. This could potentially be the result of overwhelming surface tension and persistent alveolar collapse that fails to open with deep inflation and increasing PEEP.[23,24] The reduction in total elastance and partial restoration of PEEP responsiveness in the decellularized lungs after the addition of exogenous surfactant supports this latter assertion This suggests that temporal changes in lung elastance could be used to assess changes in surface tension attributable to recovered surfactant production after tissue engraftment. This approach will be useful in assessing for differentiation of cells cultured in the decellularized lungs by providing a functional assessment of surface tension and a surrogate measure of surfactant function/production, which will complement existing histologic methods of identifying surfactant protein.

Combining information from analyses of immunofluorescent staining, western blot, and MS, we demonstrated that key ECM proteins, including collagen I, collagen IV, laminin, and fibronectin, were preserved but that there was substantial loss of GAG and elastin in the decellularization process. These results are similar to other recent descriptions of lung decellularization utilizing detergent-based protocols but with better preservation of fibronectin and more marked decreased in elastin.[16–19] However, we also observed that saline treatment of the control lungs decreased relative levels of fibronectin and elastin as demonstrated by western blots. Control lungs were incubated in saline solution not only as a detergent diluent control, but also as a control for temperature, because the decellularization process occurs at 4°C and at room temperature over multiple days. The increased relative expression of fibronectin and elastin in the

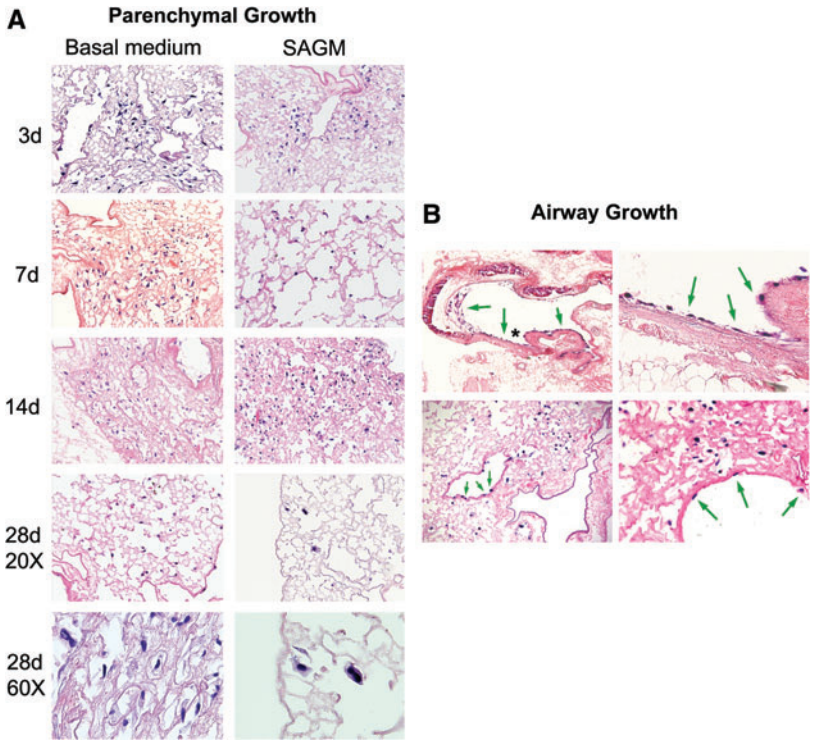

FIG. 5. Intratracheally inoculated MSCs cultured up to 1 month in both basal MSC media and in SAGM grow in parenchymal and airway regions of decellularized whole mouse lungs. Representative photomicrographs depict MSCs in parenchymal lung regions **(A)** and in airways **(B)**. High power images demonstrate several morphologies of MSCs growing in parenchymal lung regions for 7 days in basal medium (top row) or 14 days in SAGM (bottom row) **(A)**. Green arrows highlight cells growing in airways, and the asterisk in the upper left-hand image show the region magnified in the upper right-hand image. Original magnifications in **(A)** are 200×, except 600× where indicated by label "60×"; beginning in upper left-hand corner and proceeding clockwise. Original magnifications in **(B)** are 100×, 400×, 400×, and 200×. **(C)** Ki67 immunofluorescence (red) of MSCs cultured in either basal MSC medium or in SAGM demonstrates widespread expression in the majority of cells 14 days after intratracheal inoculation into decellularized mouse lungs. Representative photomicrographs are shown with DAPI nuclear costaining (original magnification 400×). **(D)** Total RNA in homogenates of whole decellularized lungs increases over time after inoculation with MSCs and culture in basal MSC media but decreases with culture in SAGM. Values represent means ± standard error of the means of three lungs evaluated for each experimental condition. *$p \le 0.05$, **$p \le 0.005$, ***$p \le 0.0005$. **(E)** Relative mRNA expression for selected genes is depicted. Values represent means ± standard error of the means of three lungs per experimental condition. *$p \le 0.05$, **$p \le 0.005$, ***$p \le 0.0005$. **(F)** Alizarin red staining of MSCs cultured in either basal MSC medium or in SAGM for 28 days after inoculation into whole decellularized mouse lings. Blue arrows highlight individual cells. MSCs, mesenchymal stromal cells; SAGM, small airways growth media. Color images available online at www.liebertonline.com/tea

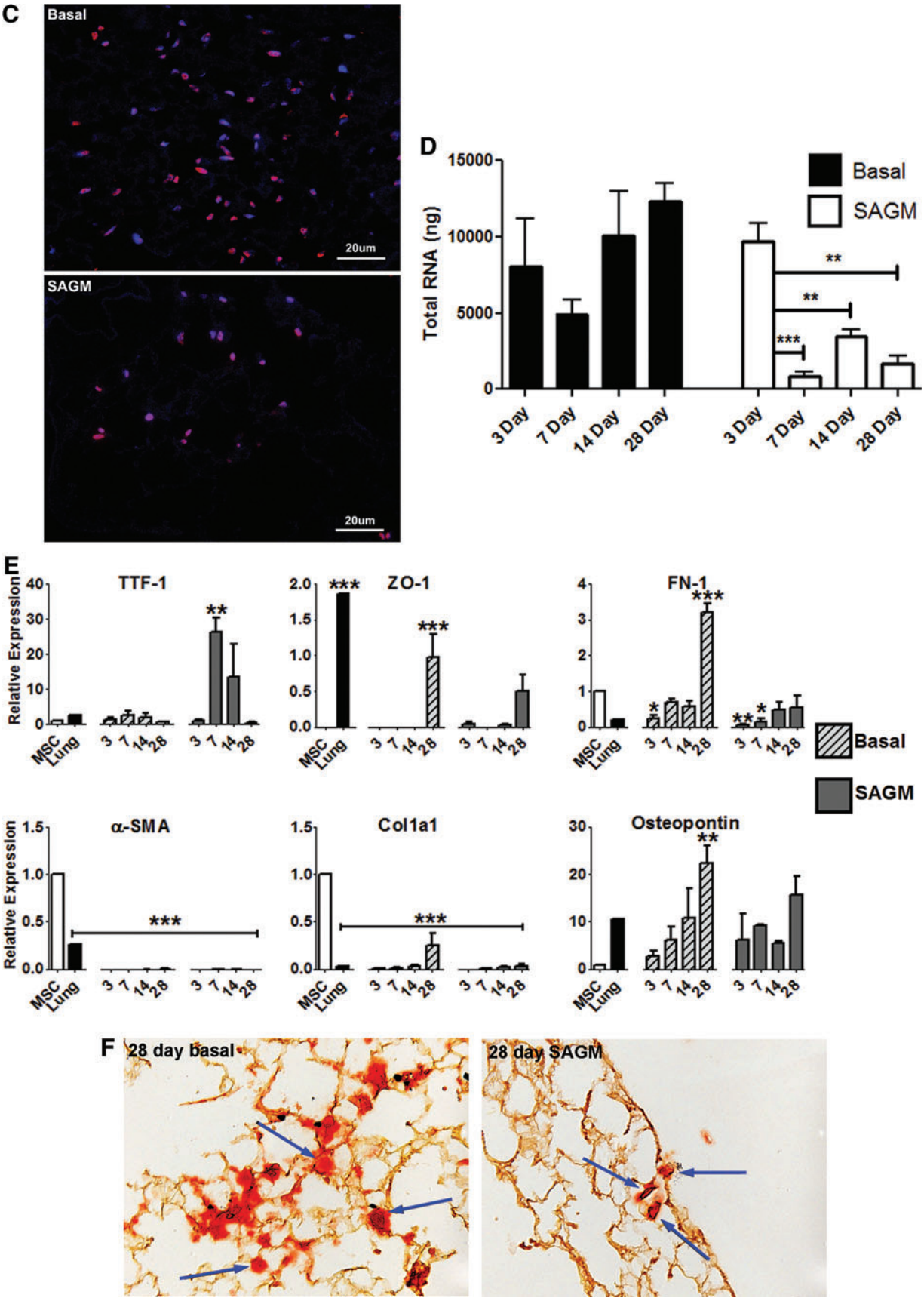

FIG. 5. (Continued).

decellularized lungs compared with naive lungs is similar to that observed with other ECM proteins including laminin and the collagens as these ECM proteins now represent a greater proportion of total protein following removal of most, but not all, cytosolic, nuclear, and cytoskeletal proteins during the decellularization process. The triple helical and highly crosslinked nature of collagens likely protects these molecules from temperature- or salt-mediated disruption. One would expect that laminin and fibronectin would be equally affected by salt-mediated dissociation from their interaction with plasma membrane integrin receptors and that elastin would be the most affected. However, only fibronectin and elastin expression decreased in saline-treated lungs. At this point, we are not completely clear as to why this occurred but speculate that fibronectin and elastin might be more susceptible to matrix metalloproteinase (MMP)-

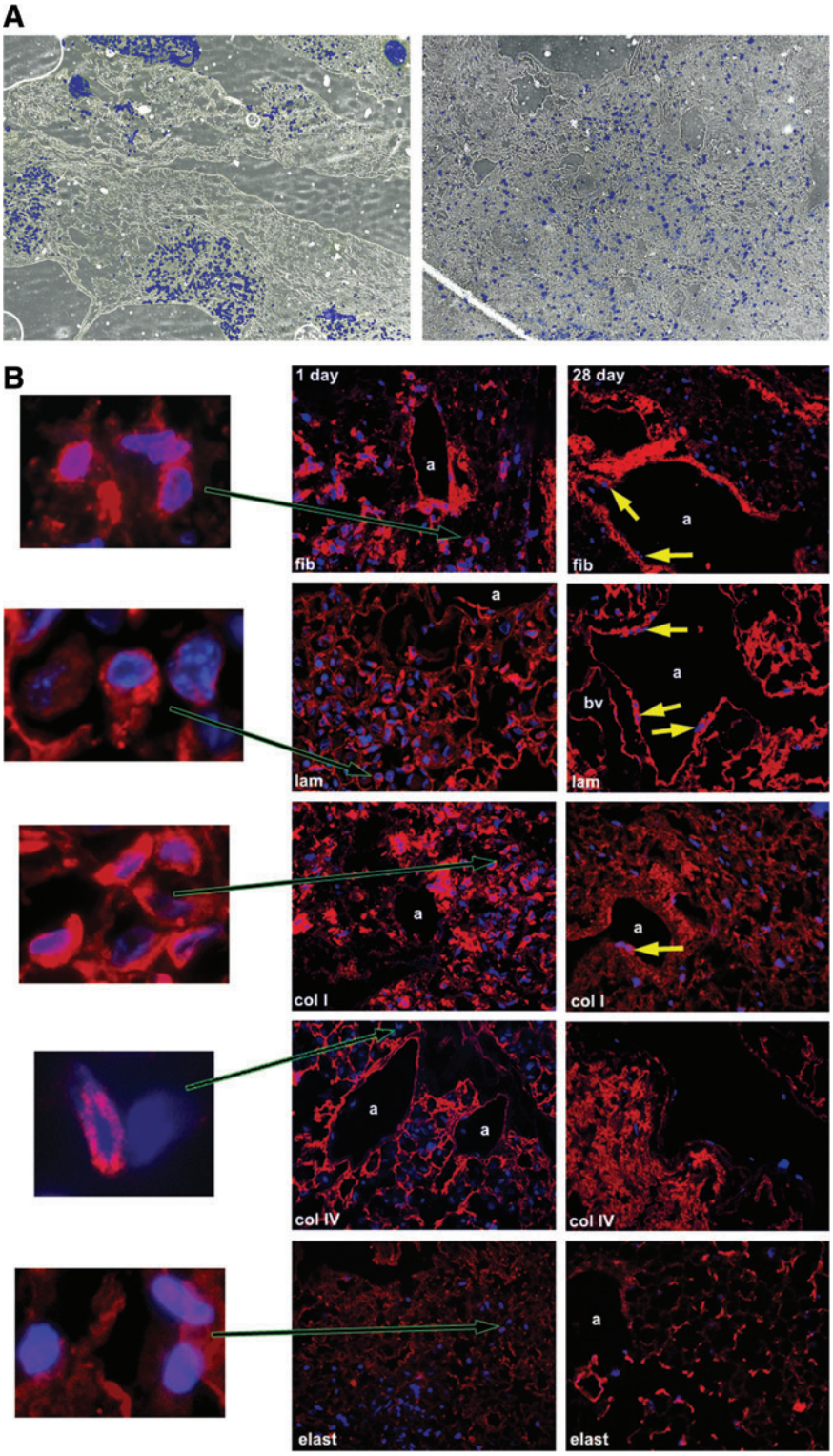

FIG. 6. MSCs inoculated into decellularized mouse lungs initially localize to regions enriched in fibronectin, laminin, type I collagen, and type IV collagen but do not proliferate in fibronectin-rich regions after 28 days in culture. **(A)** MSCs are localized in clumps 1 day after intratracheal inoculation but spread throughout the parenchyma and along airways 28 days after culture in basal MSC medium. Representative colorized phase contrast images are shown. Original magnification 50×. **(B)** Representative photomicrographs obtained 1 and 28 days after MSC inoculation into decellularized whole mouse lungs. For each panel, specific ECM protein immunofluorescence is depicted in red with DAPI nuclear costaining. Enlargements demonstrate that MSCs also produce fibronectin, laminin, and collagen I but not collagen IV or elastin after either 1 or 28 days in culture. **(C)** Representative photomicrographs demonstrating a different pattern of initial localization of inoculated C10 mouse lung epithelial cells with respect to fibronectin as compared to MSCs. Further, blocking the α5 integrin on MSCs with a neutralizing antibody prior to cell inoculation also results in MSCs localizing in areas not enriched in fibronectin. Enlargements demonstrate that the C10 cells themselves may produce small amounts of fibronectin whereas MSCs incubated with the neutralizing antibody do not appear to make fibronectin. a, airways; bv, blood vessels; fn, fibronectin; lam, laminin; elast, elastin; colI, type I collagen; colIV, type IV collagen. Yellow arrows depict MSCs growing along airway walls. Original magnifications 400×. Color images available online at www.liebertonline.com/tea

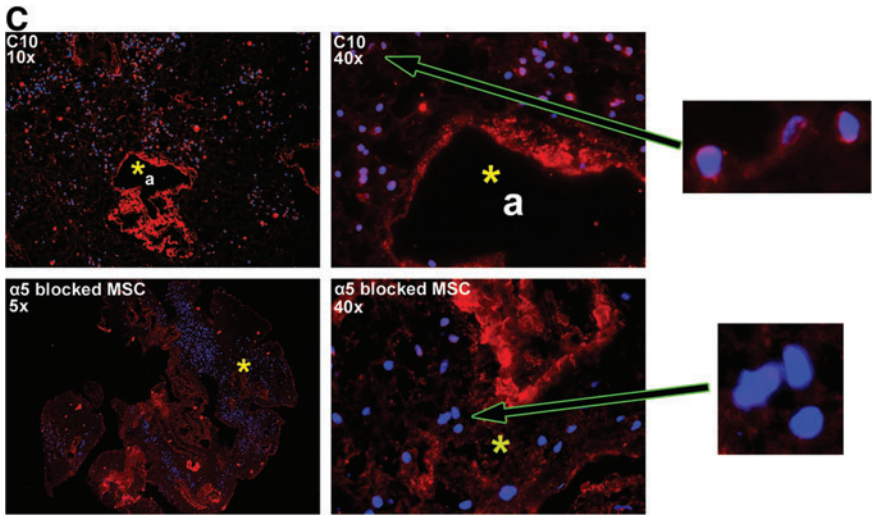

FIG. 6. (Continued).

mediated proteolysis activated during the decellularization process. Studies are currently in progress to characterize MMP-mediated proteolysis at each step of decellularization stimulated by saline and by different detergents. Nonetheless these results highlight that analyses of saline-treated lungs, temperature effects, and other factors such as length of storage time on the integrity and composition of the ECM proteins remaining in the decellularized lungs is critical to optimize decellularization and subsequent recellularization.

The enhanced chemiluminescence-based western blot method is more sensitive than either immunohistochemistry or mass spectrometry. We doubt that the immunohistochemical labeling is due to nonspecific staining as the elastin antibody recognized a single immunoreactive species on the western blot. Further, we have no reason to believe that the processing for mass spectrometry somehow only selectively eliminated elastin. Therefore, the different results obtained by mass spectrometry and antibody based methods is primarily due to sensitivity of detect and substantiates our comprehensive use of all three approaches.

In addition to clarifying the composition and distribution of remaining ECM proteins, these combined analyses demonstrated a wide range of intracellular structural proteins and enzymes remaining in the decellularized lungs. As more soluble intracellular proteins are largely removed, those proteins that remain are presumably more adherent or sticky, notably actin and myosin. It is unknown whether the presence of these residual intracellular proteins might influence the initial binding and growth of cells inoculated into the decellularized lung scaffolds or, further, potentially trigger immune responses after *in vivo* implantation.

Recellularization of decellularized whole rat lungs with mixtures of fetal rat lung homogenate, endothelial cells, and alveolar epithelial carcinoma cells in two recent studies has yielded promising results.[18,19] Although the cellular architecture resulting from these studies did not fully resemble that of native lung, the recellularized lungs sustained a degree of gas exchange and vascular perfusion over short periods when surgically implanted in live rats.[18,19] These studies illustrate the potential for differentiated adult epithelial, vascular, and interstitial lung cells to recellularize lung scaffolds; however, the potential of stem or progenitor cells has yet to be fully evaluated. Several studies of ESCs, adult stem cells, and adult progenitor cells cultured in synthetic scaffolds have yielded intriguing results. When cultured in synthetic polymer constructs and implanted subcutaneously in nude mice or in sheep thoracic cavities, putative somatic progenitor cells isolated from adult sheep lungs increased expression of airway and alveolar epithelial markers and developed into structures resembling lung airways and parenchyma.[33] Implantation of adult sheep lung-derived MSCs cultured in synthetic fibronectin-hydrogel scaffolds into lungs of sheep with experimentally induced emphysema resulted in improved tissue mass and lung perfusion.[33,34] Murine ESCs inoculated into decellularized rat lungs apparently differentiated into cells that expressed phenotypic markers of epithelial and vascular structures.[17] These studies suggest the utility of artificial scaffolds, including whole decellularized lungs, for investigation of stem and progenitor cell growth and differentiation into lung tissue. However, many questions remain about the capacity of the myriad stem- and progenitor-cell types to differentiate upon inoculation into biologically derived matrix. Elucidating the differences between these lines and the mechanisms by which they can be induced to form functional tissue will prove vital in growing organs *ex vivo*.

We utilized MSCs in these studies for two reasons. Foremost, published data, including our own[35–38] demonstrates that MSCs can be induced to acquire the phenotype of lung airway and alveolar cells. This occurs both *in vitro* in standard tissue culture dishes and also *in vivo* following systemic (intravenous) administration to mice. We had thus hoped that inoculation of the MSCs into the decellularized lungs would also result in acquisition of lung epithelial phenotype. As such, this would provide a strong case for potential use of MSCs in lung recellularization strategies. The second reason for use of MSCs is that they have been extensively studied both in our laboratory and in other laboratories and thus provide a very useful adult stem cell type for developing and validating the various analytical approaches highlighted in these studies.

We found that mouse bone marrow-derived MSCs readily adhered to the residual ECM after intratracheal inoculation into decellularized whole mouse lungs. When assessed 1 day after inoculation, most cells were clustered together and were associated in regions enriched in collagens I and IV, laminin, and fibronectin. This suggests that MSCs exhibit preferential adherence to these ECM proteins, which is likely driven by interaction of MSC cell surface integrins with ligands found in the ECM.[39,40] After 28 days in culture, MSCs spread more diffusely throughout the lung and appeared to grow in regions enriched in type I collagen, type IV collagen, and laminin but not in fibronectin. This observation suggests that while fibronectin may be important for initial adherence, subsequent growth is more dependent on interactions with the other ECM proteins. Importantly, this appears not to be random distribution of the inoculated MSCs as intratracheal administration of C10 mouse lung epithelial cells, which express different cell surface integrins than MSCs and notably do not constitutively express the major fibronectin-binding integrin, $\alpha5\beta1$, results in a different initial distribution pattern.[25] Further preincubation of the MSCs with a blocking anti $\alpha5$ integrin antibody, which inhibits binding of the cells to fibronectin, inhibits the initial localization of the inoculated MSCs to fibronectin-rich areas. Interestingly, use of this antibody also appears to inhibit fibronectin production by the inoculated MSCs. This phenomenon has been previously described[41] and will be the basis of further studies attempting to differentiate the respective roles of ECM proteins produced by inoculated cells versus those remaining in the decellularized lungs. Understanding of initial binding determinants and those important for growth and differentiation will be critical for directing and optimizing patterns of recellularization of the decellularized lungs.

MSCs cultured in basal MSC medium in the decellularized lungs appeared to increase in number over 1 month, whereas cells cultured in SAGM decreased, as approximated by amount of total RNA extracted per recellularized lung. Since most cells, including those cultured in SAGM, expressed the proliferation marker Ki67 and did not express the early apoptosis marker Caspase 3 at all time points, the reason for this decrease in cell number is unclear. We hypothesize that the net decrease in MSCs grown in SAGM media may be due to either activation of an alternative cell death pathway which is caspase 3 independent (possibly apoptosis-inducing-factor dependent) or that we are missing a transient state of caspase-3 activation by staining over multiday intervals. These hypotheses are currently being further investigated. However, we don't believe that overall decrease in cell number is due to the MSCs undergoing a massive extinction event, which would be noticeable via staining. Rather it seems that a small number of cells die in a gradual fashion. We also didn't observe cells clustered around the external pleural surface of the inoculated lungs suggesting that the cells are not migrating out of the lung.

Culture in SAGM, which contains human recombinant EGF, can induce expression of several airway and alveolar epithelial genes and can also induce vascular endothelial gene expression in MSCs cultured in plastic tissue culture dishes.[35] However, this phenomenon occurs only rarely after *in vivo* administration of MSCs under a variety of experimental conditions.[35,36] In the present study, apart from transient expression of the early lung developmental marker TTF-1, MSCs did not up-regulate genes typically expressed by airway epithelium, alveolar epithelium, or pulmonary vascular endothelium after culture in either growth medium. However, the lung scaffolds in this study were neither ventilated nor perfused during culture, conditions that could potentially alter the growth and differentiation of inoculated MSCs.[6,7] Intravascular inoculation of MSCs, in parallel with the intratracheal approach investigated here, could also affect growth and differentiation patterns. Although MSCs did not express genes typical to cells found in lung tissue, they did express osteopontin mRNA and some cells stained positively with Alizarin Red when cultured in either basal MSC medium or SAGM, suggestive of differentiation along the osteoblast lineage. As osteoblastic cells are not found in normal lung, further study is required to understand why this occurred and to manipulate the culture environment so that osteoblastic differentiation is not promoted. No markers characteristic of differentiation along adipocyte or chondrocyte lineages were produced by the MSCs under these conditions. The MSCs expressed MSC-associated genes and produced collagen I, fibronectin, and laminin throughout culture in the decellularized lungs in the presence of basal MSC media. Thus, it appears that MSCs can retain mesenchymal phenotype within a 3D ECM protein scaffold reminiscent of native lung and secrete ECM proteins that contribute to the scaffold. This suggests a potential utility of inoculating MSCs into lung scaffolds to lay a physical foundation (ECM) for subsequent inoculation of other cell types and also as a means of blunting potential immune responses to any retained intracellular proteins.

Conclusion

These studies demonstrate that decellularized whole lungs are powerful tools with which to investigate recellularization and development of functional lung tissue from stem and progenitor cell populations. Further characterization of the decellularization and recellularization of whole lungs will provide a robust means of achieving the ultimate goal of generating functional lung tissue *ex vivo* that can be used for surgical implantation.

Acknowledgments

The authors gratefully acknowledge Lennart Lundblad, Nirav Daphthary, and Minara Aliyeva for assistance with assessments of lung mechanics, Stephen Bell for assistance with perfusion assessments, Holly Stradecki for assistance with western blot analyses, Marilyn Wadworth for assistance with immunohistochemistry, Nicole Bishop for electron microscopic analyses, Svitlana Danchuk and Sergiy Sukhanov for assistance in analyses of eGFP-positive and control C57Bl/6 mouse lungs, Michael Sullivan with computer analyses, the staffs of the Offices of Animal Care Management at the University of Vermont and at Tulane, and Bruce Bunnell, Christine Finck, Andrew Hoffman, and Brenda Ogle for critical reads of the article.

Disclosure Statement

No competing financial interests exist.

References

1. Bhatia, S.K. Tissue engineering for clinical applications. Biotechnol J **5,** 1309, 2010.

2. Ott, H.C., Matthiesen, T.S., Goh, S.K., Black, L.D., Kren, S.M., Netoff, T.I., and Taylor, D.A. Perfusion-decellularized matrix: using nature's platform to engineer a bioartificial heart. Nature Med **14,** 213, 2008.
3. Uygun, B.E., Soto-Gutierrez, A., Yagi, H., Izamis, M.L., Guzzardi, M.A., Shulman, C., Milwid, J., Kobayashi, N., Tilles, A., Berthiaume, F., Hertl, M., Nahmias, Y., Yarmush, M.L., and Uygun, K. Organ reengineering through development of a transplantable recellularized liver graft using decellularized liver matrix. Nat Med **16,** 814, 2010.
4. Mondrinos, M.J., Koutzaki, S., Lelkes, P.I., and Finck, C.M. A tissue-engineered model of fetal distal lung tissue. Am J Physiol Lung Cell Mol Physiol **293,** L639, 2007.
5. Lin, Y.M., Boccaccini, A.R., Polak, J.M., Bishop, A.E., and Maquet, V. Biocompatibility of poly-DL-lactic acid (PDLLA) for lung tissue engineering. J Biomater Appl **21,** 109, 2005.
6. Choe, M.M., Sporn, P.H., and Swartz, M.A. Extracellular matrix remodeling by dynamic strain in a three-dimensional tissue-engineered human airway wall model. Am J Respir Cell Mol Biol **35,** 306, 2006.
7. Liu, M., Xu, J., Souza, P., Tanswell, B., Tanswell, A.K., and Post, M. The effect of mechanical strain on fetal rat lung cell proliferation: comparison of two- and three-dimensional culture systems. In Vitro Cell Dev Biol Anim **31,** 858, 1995.
8. Andrade, C.F., Wong, A.P., Waddell, T.K., Keshavjee, S., and Liu, M. Cell-based tissue engineering for lung regeneration. Am J Physiol Lung Cell Mol Physiol **292,** L510, 2007.
9. Hoganson, D.M., Pryor, H.I., II, and Vacanti, J.P. Tissue engineering and organ structure: a vascularized approach to liver and lung. Pediatr Res **63,** 520, 2008.
10. Mondrinos, M.J., Koutzaki, S.H., Poblete, H.M., Crisanti, M.C., Lelkes, P.I., and Finck, C.M. In vivo pulmonary tissue engineering: contribution of donor-derived endothelial cells to construct vascularization. Tissue Eng Part A **14,** 361, 2008.
11. Antunes, M.B., Woodworth, B.J., Bhargave, G., Xiong, G., Aguilar, J.L., Ratner, A.J., Kreindler, J.L., Rubenstein, R.C., and Cohen, N.A. Murine nasal septa for respiratory epithelial air-liquid interface cultures. Biotechniques **43,** 195, 2007.
12. Gilbert, T.W., Gilbert, S., Madden, M., Reynolds, S.D., and Badylak, S.F. Morphologic assessment of extracellular matrix scaffolds for patch tracheoplasty in a canine model. Ann Thorac Surg **86,** 967, 2008.
13. Macchiarini, P., *et al.* Clinical transplantation of a tissue-engineered airway. Lancet **372**, 2023, 2008.
14. Panoskaltsis-Mortari, A., and Weiss, D.J. Breathing new life into lung transplantation therapy. Mol Ther **18,** 1581, 2010.
15. Lwebuga-Mukasa, J.S., Ingbar, D.H., and Madri, J.A. Repopulation of a human alveolar matrix by adult rat type ll penumocytes *in vitro*. Exp Lung Res **162,** 423, 1986.
16. Price, A.P., *et al.* Development of a decellularized lung bioreactor system for bioengineering the lung: the matrix reloaded. Tissue Eng Part A, **16,** 2581, 2010.
17. Cortiella, J., *et al.* Influence of acellular natural lung matrix on murine embryonic stem cell differentiation and tissue formation. Tissue Eng Part A **16,** 2565, 2010.
18. Petersen, T.H., *et al.* Tissue-engineered lungs for *in vivo* implantation. Science **329,** 538, 2010.
19. Ott, H.C., Clippinger, B., Conrad, C., Schuetz, C., Pomerantseva, I., Ikonomou, L., Kotton, D., and Vacanti, J.P. Regeneration and orthotopic transplantation of a bioartificial lung. Nat Med **16,** 927, 2010.
20. Sekiya, I., Larson, B.L., Smith, J.R., Pochampally, R., Cui, J.G., and Prockop, D.J. Expansion of human adult stem cells from bone marrow stroma: conditions that maximize the yields of early progenitors and evaluate their quality. Stem Cells **20,** 530, 2002.
21. Lluri, G., Langlois, G.D., Soloway, P.D., and Jaworski, D.M. Tissue inhibitor of metalloproteinase-2 (TIMP-2) regulates myogenesis and beta1 integrin expression *in vitro*. Exp Cell Res **314,** 11, 2008.
22. Gomes, R.F., Shardonofsky, F., Eidelman, D.H., and Bates, J.H.T. Respiratory mechanics and lung development in the rat from early age to adulthood. J Appl Physiol **90,** 1631, 2001.
23. Allen, G.B., Suratt, B.T., Rinaldi, L., Petty, J.M., and Bates, J.H. Choosing the frequency of deep inflation in mice: balancing recruitment against ventilator-induced lung injury. Am J Physiol Lung Cell Mol Physiol **291,** L710, 2006.
24. Allen, G.B., Pavone, L.A., DiRocco, J.D., Bates, J.H.T., and Nieman, G.F. Pulmonary impedance and alveolar instability during injurious ventilation in rats. J Appl Physiol **99,** 723, 2005.
25. Malkinson, A.M., Dwyer-Nield, L.D., Rice, P.L., and Dinsdale, D. Mouse lung epithelial cell lines—tools for the study of differentiation and the neoplastic phenotype. Toxicology **123**, 53, 1997.
26. You, Y., Richer, E.J., Huang, T., and Brody, S.L., Growth and differentiation of mouse tracheal epithelial cells: selection of a proliferative population. Am J Physiol Lung Cell Mol Physiol **283,** L1315, 2002.
27. Zar, J. Biostatistical Analysis. Upper Saddle River, NJ: Prentice-Hall, Inc., 1974.
28. Orens, J.B., and Garrity, E.R. General overview of lung transplantation and review of organ allocation. Proc Am Thorac Soc **6,** 13, 2009.
29. Ahsan, T., and Nerem, R.M. Fluid shear stress promotes an endothelial-like phenotype during the early differentiation of embryonic stem cells. Tissue Eng Part A, **16,** 3547, 2010.
30. Hewitt, K.J., Shamis, Y., Carlson, M.W., Aberdam, E., Aberdam, D., and Garlick, J.A. Three-dimensional epithelial tissues generated from human embryonic stem cells. Tissue Eng Part A **15,** 3417, 2009.
31. Lin, Y.M., Zhang, A., Rippon, H.J., Bismarck, A., and Bishop, A.E. Tissue engineering of lung: the effect of extracellular matrix on the differentiation of embryonic stem cells to pneumocytes. Tissue Eng Part A **16,** 1515, 2010.
32. Wang, Y., Wong, L.B., and Mao, H. Induction of ciliated cells from avian embryonic stem cells using three-dimensional matrix. Tissue Eng Part C **16,** 929, 2010.
33. Ingenito, E.P., Sen, E., Tsai, L.W., Murthy, S., and Hoffman, A. Design and testing of biological scaffolds for delivering reparative cells to target sites in the lung. J Tissue Eng Regen Med **4,** 259, 2010.
34. Ingenito, E.P., Tsai, L., Murthy, S., Tyagi, S., Mazan, M., and Hoffman, A. Autologous lung-derived mesenchymal stem cell transplantation in experimental emphysema. Cell Transplant 2011 [Epub ahead of print]; DOI: 10.3727/096368910X550233.
35. Sueblinvong, V., Loi, R., Eisenhauer, P.L., Bernstein, I.M., Suratt, B.T., Spees, J.L., and Weiss, D.J. Derivation of lung epithelium from human cord blood-derived mesenchymal stem cells. Am J Resp Crit Care Med **177,** 701, 2008.
36. Loi, R., Beckett, T., Goncz, K.K., Suratt, B.T., and Weiss, D.J. Limited restoration of cystic fibrosis lung epithelium *in vivo* with adult marrow derived cells. Am J Resp Crit Care Med **173,** 171, 2006.
37. Wang, G., *et al.* Adult stem cells from bone marrow stroma differentiate into airway epithelial cells: potential therapy for cystic fibrosis. Proc Natl Acad Sci U S A **102,** 186, 2005.

38. Xu, J., *et al.* Prevention of endotoxin-induced systemic response by bone marrow-derived mesenchymal stem cells in mice. Am J Physiol Lung Cell Mol Physiol **293,** L131, 2007.
39. Semon, J.A., Nagy, L.H., Llamas, C.B., Tucker, H.A., Lee, R.H., and Prockop, D.J. Integrin expression and integrin-mediated adhesion *in vitro* of multopotent stromal cells (MSCs) to endothelial cells from various blood vessels. Cell Tissue Res **341,** 147, 2010.
40. Ellis, S.J., and Tanentzapf, G. Integrin-mediated adhesion and stem cell-niche interactions. Cell Tissue Res **339,** 121, 2010.
41. Singh, P., *et al.* Assembly of fibronectin extracellular matrix. Annu Rev Cell Dev Biol **26,** 397, 2010.

Address correspondence to:
Daniel J. Weiss, M.D., Ph.D.
Department of Medicine
University of Vermont College of Medicine
226 Health Science Research Facility
Burlington, VT 05405

E-mail: dweiss@uvm.edu

Received: May 24, 2011
Accepted: July 12, 2011
Online Publication Date: September 22, 2011